Incomplete mixing and reactions in laminar shear flow

A. Paster*
School of Mechanical Engineering, Faculty of Engineering, Tel Aviv University, Tel Aviv 69978, Israel

T. Aquino† and D. Bolster‡
Department of Civil and Environmental Engineering and Earth Sciences, University of Notre Dame, Notre Dame, Indiana 46556, USA
(Received 13 April 2015; published 31 July 2015)

Incomplete mixing of reactive solutes is well known to slow down reaction rates relative to what would be expected from assuming perfect mixing. In purely diffusive systems, for example, it is known that small initial fluctuations in reactant concentrations can lead to reactant segregation, which in the long run can reduce global reaction rates due to poor mixing. In contrast, nonuniform flows can enhance mixing between interacting solutes. Thus, a natural question arises: Can nonuniform flows sufficiently enhance mixing to restrain incomplete mixing effects and, if so, under what conditions? We address this question by considering a specific and simple case, namely, a laminar pure shear reactive flow. Two solution approaches are developed: a Lagrangian random walk method and a semianalytical solution. The results consistently highlight that if shear effects in the system are not sufficiently strong, incomplete mixing effects initially similar to purely diffusive systems will occur, slowing down the overall reaction rate. Then, at some later time, dependent on the strength of the shear, the system will return to behaving as if it were well mixed, but represented by a reduced effective reaction rate.

DOI: 10.1103/PhysRevE.92.012922 PACS number(s): 82.40.Ck, 05.10.Gg, 05.10.Ln, 47.70.Fw

I. INTRODUCTION

Chemical reactions driven by mixing are important processes that occur in a wide variety of engineered and natural flows. Some common examples of practical interest include atmospheric flows [1], oceanographic flows [2], riverine flows [3], limnologic flows [4] and industrial reactors [5], to mention but a few. One of the perhaps most obvious but critical features to recognize in any reactive system is that in order for reactions to actually occur, the chemicals involved in the reaction must physically come into contact with one another. Mixing is the physical process that enables this contact to occur. In flowing systems, this is inherently a fluid dynamics problem as flows can act in such a way as to enhance, or indeed suppress, mixing and thus chemical reactions.

While it is broadly recognized that nonuniform flows can enhance mixing, there is increasing evidence that current models do not adequately characterize these mixing processes, often overestimating reaction rates relative to what is observed in field and laboratory experiments [6–13]. This is likely due to the fundamental difference between the enhanced spreading and stretching of solutes that nonuniform flows induce, as quantified, for example, by an effective dispersion coefficient, and the true degree of mixing that actually occurs [14]. While spreading and mixing are intricately related and indeed historically the words have been used interchangeably, it is important to highlight that they are different processes. This is because spreading may not account for subscale fluctuations in concentrations that are critical to understanding mixing. Thus, there is a need for improved models that can accurately capture the nature of reactive transport. In this work, we argue that Lagrangian-based approaches are naturally conducive to capturing these effects. To understand this issue in greater detail we focus on the irreversible bimolecular reaction $A + B \rightarrow P$, which can be regarded as the fundamental building block of more complex reaction chains (see Ref. [15] for a detailed discussion).

A rich body of literature exists exploring the effects of incomplete mixing on reactions in purely diffusive systems [16–21]. Consider the following classical experiment where a domain is initially filled with equal total amounts of A and B, such that $C_A(x,t=0) = C_B(x,t=0) = C_0$, where A and B move by diffusion and react with one another kinetically with some known rate coefficient k. For this setup, there is an analytical solution $C_A(x,t) = C_B(x,t) = C_0/(1+kC_0t)$, which at late times scales like inverse time, or t^{-1}. It is important to note that this analytical solution relies implicitly on the assumption that the concentrations are completely uniform and equal in space, or in other words that they are always well mixed. If, however, there is some stochastic fluctuation of the concentration fields around their mean value, this late-time scaling will break down. For such systems, it has been shown that the late-time mean concentration of the species will scale as $t^{-d/4}$ where d is the number of spatial dimensions in the system under consideration [18,21]. Stochastic fluctuations are ubiquitous in real systems and so such breakdowns should perhaps be regarded as the norm rather than the exception.

Specifically, for such systems, at early times, fluctuations about the mean concentration are often small enough to be discarded and the system behaves as is if it were indeed well mixed. However, due to the fact that reactions consume mass, as the mean concentrations become smaller, the relative influence of the fluctuations becomes increasingly important. Indeed, at late times isolated pockets, or so-called segregated *islands*, of each reactive constituent emerge and the reaction is limited by how quickly reactants can diffuse across the interfaces of these islands, resulting in the slower $t^{-d/4}$ scaling [16–18,21]. This phenomenon often goes by the name of

*paster@tau.ac.il
†tdecampo@nd.edu
‡dbolster@nd.edu

Ovchinnikov-Zeldovich segregation and this behavior has been observed experimentally [19,20].

This problem has also received a great deal of attention in systems where transport is not by local Fickian diffusion, but rather by anomalous dispersive transport, including nonlocal in space superdiffusive systems and nonlocal in time subdiffusive systems [22–24]. Such nonlocal transport is common in a broad array of disciplines including transport in porous media [25–27], streams [28], groundwater systems [29,30], and biological systems [31], to name a few. In all cases, similar late-time scalings for the mean concentration that deviate from the well-mixed t^{-1} scaling have been predicted and observed. The specific late-time scaling will depend on the nature of the transport and the dimensionality of the problem being considered. However, to our knowledge, this problem has received limited attention in the context where transport is by advection and diffusion in a nonuniform velocity field. As noted above, it is well known that nonuniform velocity fields can significantly affect the nature of mixing and thus can in principle strongly impact mixing-driven reactions.

While much focus has been given to mixing in turbulent flows, it is important to recognize that mixing in nonuniform laminar flows can also result in very interesting mixing dynamics [32–38]. In this work, we propose to study this problem in one of the simplest forms of nonuniform flow, namely, a pure laminar shear flow. Pure shear flows have received a great deal of attention in a variety of applications due to both their simplicity and ability to provide invaluable physical insight. Okubo [39,40] studied transport in pure shear flows to better understand solute dispersion in rivers, estuaries, lakes, and oceans. Novikov [41] used it as a model to study turbulent dispersion in streams. Others [42–44] highlight it as an important case in understanding turbulent dispersion. More recently, it was shown [45] that from purely a mixing perspective, as quantified by the scalar dissipation rate [46,47] or dilution index [48], a pure shear flow is incredibly efficient at mixing. The term *hypermixing* was used, emphasizing that the predicted mixing is even faster than conventional superdiffusion. Reference [49] extended this to more complex flows using the Okubo-Weiss metric to quantify enhancement of mixing due to more general locally nonuniform velocity fields.

The above discussion leads us the ask the following question: Is mixing in a laminar shear flow sufficient to overcome incomplete mixing effects on the evolution of mean concentration in a reactive system or will incomplete mixing effects still persist? The answer to this question is addressed in this paper with an application to a nonuniform flow of a random walk particle tracking method designed for reactive transport. It was originally developed for purely diffusive transport [50] and we extend it further. The results of this paper provide a general understanding of the influence of shear flows on incomplete mixing, paving the road for more general nonuniform velocity fields.

The paper is structured as follows. In Sec. II we present the governing equations for flow, transport, and reaction for the chosen setup in dimensional and nondimensional forms. In Sec. III we discuss the initial conditions, focusing on both deterministic and stochastic initial conditions, which are at the root of incomplete mixing. In Sec. IV we describe the Lagrangian random walk particle tracking method for reactive transport. In Sec. V we present and discuss results obtained with this method. In Sec. VI we propose a semianalytical model to interpret observations from Sec. V. We conclude with a discussion in Sec. VII.

II. GOVERNING EQUATIONS

We consider a bimolecular reactive system that is embedded in a uniform shear flow. Transport of the species is driven by a constant diffusion coefficient and advection according to the uniform shear flow. The two constituents in this system, A and B, react kinetically and irreversibly with one another, i.e., $A + B \rightarrow P$. At this point, we are not interested in what happens to the product P, but rather on how A and B are consumed, so the fate of P is neglected in this work. The flow in the system is completely independent of the transport, i.e., the flow is not affected by the concentration of the constituents. For an infinite two-dimensional space, the governing equation for transport is the advection-dispersion-reaction equation (ADRE), given for each of the species $i = A, B$ by

$$\frac{\partial C_i}{\partial t} + \alpha y \frac{\partial C_i}{\partial x} = \nabla \cdot (D \nabla C_i) - r_i, \tag{1}$$

where $C_i(\mathbf{x},t)$ is the concentration [mol L^{-d}], α is the shear rate [T^{-1}], D is the dispersion coefficient [$\mathrm{L}^2\mathrm{T}^{-1}$], assumed constant herein.

The sink term, in our case, is the local rate of reaction, and is identical for A and B since they are consumed with a 1:1 stoichiometry ratio, i.e.,

$$r_A = r_B = r\ . \tag{2}$$

We assume the law of mass action prevails for our system, and write the reaction rate as

$$r(C_A, C_B) = k C_A C_B\ , \tag{3}$$

where k [L^d mol^{-1} T^{-1}] is the kinetic rate constant for a given reaction. Thus, Eq. (1) represents a coupled set.

A. Nondimensional equations

We consider the following dimensionless variables:

$$\begin{aligned} &C^* = C/C_0, \quad t^* = kC_0 t, \quad \alpha^* = \alpha/(kC_0), \\ &x^* = x/l, \quad y^* = y/l, \end{aligned} \tag{4}$$

where l is a characteristic length associated with the initial fluctuations in concentration (e.g., a correlation length). Using these nondimensional variables, our governing equation for transport becomes

$$\frac{\partial C_i^*}{\partial t^*} + \alpha^* y^* \frac{\partial C_i^*}{\partial x^*} = \frac{1}{\mathrm{Da}} \nabla^{*2} C_i^* - C_A^* C_B^*, \tag{5}$$

where $\mathrm{Da} = \frac{kC_0 l^2}{D}$ is the Damköhler number, which quantifies the relative importance of reaction to transport by diffusion. In other words, it quantifies how quickly reactions happen relative to how quickly diffusion can homogenize a patch of size l. α^* is a dimensionless shear rate that quantifies the relative importance of shear to reaction. For the sake of convenience, we drop the stars from here on, and all the variables presented are nondimensional.

III. INITIAL CONDITIONS

The focus of this work is the emergence of incomplete mixing of reactants as the system evolves, which is known to arise due to stochastic fluctuations in the concentration field [e.g., 18,21–23]. Thus, we focus on the case of a stochastic initial condition, i.e., the initial concentration comprises a mean contribution plus a stochastic or noise term. In this case, the exact concentration at a point is unknown and statistical information is available instead.

Specifically, we assume that for each of the species A and B, the stochastic initial concentration field is given by an average value plus a white noise contribution. Decomposing the concentration into mean and a perturbation, we write for $i = A, B$

$$C_i(\mathbf{x},t) = \overline{C_i}(\mathbf{x},t) + C_i'(\mathbf{x},t), \tag{6}$$

where $\overline{C}(\mathbf{x},t)$ is the ensemble mean over all possible realizations. The perturbation C_i' has zero mean. The initial condition for the mean is given in a general manner by

$$\begin{aligned} \overline{C_A}(\mathbf{x},t=0) &= C_{A0}(\mathbf{x}), \\ \overline{C_B}(\mathbf{x},t=0) &= C_{B0}(\mathbf{x}). \end{aligned} \tag{7}$$

Assuming that the initial fluctuation term is Gaussian (or that higher order moments are irrelevant), the initial condition for the perturbation concentration of species i and j is defined by the covariance structure

$$\overline{C_i'(\mathbf{x}_1,t=0)C_j'(\mathbf{x}_2,t=0)} = \mu_{ij}(\mathbf{x}_1)\delta(\mathbf{x}_1-\mathbf{x}_2), \tag{8}$$

where μ_{ij} is the white noise amplitude and δ is Dirac's delta function. The white noise or delta-correlated initial condition is tantamount to assuming a very short range correlation in the fluctuations. The delta correlation has been shown to be a good approximation of other short range correlation structures such as exponential or Gaussian [51,52] and is invoked for mathematical convenience.

In this work, we assume the system is ergodic and statistically (space) stationary, so that the mean concentration and the correlations depend only on relative position. We also assume that the species have an identical statistical structure, so that the initial mean concentrations are equal, and are given (in nondimensional form) by

$$\overline{C_A}(t=0) = \overline{C_B}(t=0) = 1. \tag{9}$$

Furthermore, we assume that the magnitudes of fluctuation variances are equal and constant in space,

$$\mu_{AA} = \mu_{BB} = \mu, \tag{10}$$

and assume the species concentration fluctuations are initially uncorrelated, i.e.,

$$\mu_{AB} = 0. \tag{11}$$

We restrict ourselves to this specific setup for a few reasons. First, this simple case provides a great deal of physical insight into the problem at hand. Second, it is straightforward to implement this set of initial conditions in a particle tracking algorithm, although more complex structures can readily be included. Third, a semianalytical approximate solution to this system, for arbitrary dimension ($d = 1,2,3$) when shear is absent ($\alpha = 0$), is available from previous work [51], and can be used for comparison with the new results. Additionally, this approximate solution can, at least qualitatively, be extended to the shear problem as will be discussed in the following.

IV. NUMERICAL PARTICLE TRACKING SIMULATIONS

In this section, we describe a Monte Carlo based particle tracking approach to finding numerical solutions for the system and equations presented so far. The approach is an extension of previous works [51,53] which were restricted to purely diffusive transport. Here, we extend the methodology to the case of uniform shear flow, with the long term goal of ultimately utilizing it to account for more complex, general flows.

The fundamental principle behind any particle tracking numerical method is to represent the concentration field by a cloud of discrete particles, representing elementary masses of solute. Time is discretized into finite time steps (not necessarily equal), and the ADRE is applied using the concept of operator splitting: in every time step, we first annihilate any particles that would react as determined by a physically based probabilistic set of laws, representing reaction in the system; second, we move all surviving particles in a manner that represents both advection and diffusion in the system following classic random walk principles. The annihilation of particles is determined according to a local reaction probability, which is made up of two components, one based on the probability that two particles can collocate, which depends entirely on transport mechanisms, and the second based on the probability that reaction occurs given that particles have collocated, determined entirely by the kinetics of the reaction. The details are described in the following. Note that in this section we focus on the evolution of the system within a single time step Δt. Hence, for simplicity, and without loss of generality, we use $t = 0$ to denote the beginning of the time step.

A. Advection and diffusion

For the case of a shear flow, consider a numerical particle that, at the beginning of a time step, is located at $\mathbf{x}(t=0) = \mathbf{x}_0$. The combined effect of shear advection and diffusion is expressed by a random jump of the particle to a new location at time t. We define f as the probability density function (PDF) of the new location, neglecting reaction. By definition, f is the solution of the advection-diffusion equation

$$\frac{\partial f}{\partial t} + \alpha y \frac{\partial f}{\partial x} = \frac{1}{\mathrm{Da}}\nabla^2 f, \tag{12}$$

for natural boundary conditions (i.e., $f \to 0$ and $\nabla f \to 0$ as $\mathbf{x} \to \infty$) and initial condition $f(\mathbf{x},t=0) = \delta(\mathbf{x}-\mathbf{x}_0)$. Hence, f is the fundamental solution of (12). It is given by the multivariate Gaussian [40,45]

$$f(\mathbf{x},t;\mathbf{x}_0) = \frac{1}{(2\pi)^{d/2}\sqrt{\det[\boldsymbol{\kappa}]}} \exp\left[-\frac{1}{2}\xi^T\boldsymbol{\kappa}^{-1}\xi\right] \tag{13}$$

with a covariance matrix given for $d = 2$ by

$$\boldsymbol{\kappa} = \boldsymbol{\kappa}(t) = \frac{2t}{\mathrm{Da}}\begin{bmatrix} 1+(\alpha t)^2/3 & \alpha t/2 \\ \alpha t/2 & 1 \end{bmatrix}, \tag{14}$$

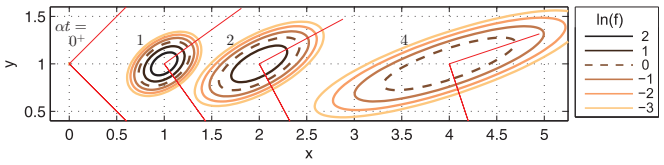

FIG. 1. (Color online) Illustration of the temporal evolution of the spatial PDF (log scale) and the eigenvectors of $\boldsymbol{\kappa}$ for a passive particle transported by shear flow.

where

$$\xi = \mathbf{x} - (\mathbf{x}_0 + \alpha y_0 t \hat{\mathbf{x}}) \tag{15}$$

is the offset from the mean location, $y_0 = \mathbf{x}_0 \cdot \hat{\mathbf{y}}$ is the initial y coordinate, and $\hat{\mathbf{x}}$, $\hat{\mathbf{y}}$ are the unit vectors in the x, y directions, respectively. Isocontours of the distribution are rotated ellipses with common foci at $\mathbf{x}_0 + \alpha y_0 t \hat{\mathbf{x}}$ (see Fig. 1). The principal axes of the ellipses are aligned with the eigenvectors of $\boldsymbol{\kappa}$, and rotate with time due to shear; one axis is growing superdiffusively and the other diffusively. Note that when $\alpha \to 0$, the distribution (13) converges to the $2d$ axisymmetric Gaussian (the fundamental solution of the ADE with constant diffusion). Further details on the implementation of this method, as well as analytical expressions for the eigenvalues and eigenvectors $\boldsymbol{\kappa}$, are provided in Appendix A.

B. Reaction

Next, based purely on transport, we wish to determine if two particles that are initially separated at $t = 0$ will collocate, and thus potentially react, over the next time step. Consider two particles, one of species A and the other of species B, that are are located at $\mathbf{x}_A, \mathbf{x}_B$ initially at $t = 0$. The temporal density of their probability to collocate over some infinitesimal volume $d\mathbf{x}$ at time t is obtained by the product of their respective random walk PDFs and $d\mathbf{x}$. Thus, the temporal density of their probability to collocate in *any* position in space is given by an integral over this product,

$$v = \int f(\mathbf{x},t;\mathbf{x}_A) f(\mathbf{x},t;\mathbf{x}_B) d\mathbf{x}, \tag{16}$$

where integration is taken over the entire space. This expression is a convolution of two Gaussians, and is itself equal to a Gaussian with the sum of variances

$$v(\mathbf{s},t) = \frac{1}{2\pi\sqrt{\det[\boldsymbol{\kappa}_A + \boldsymbol{\kappa}_B]}} \exp\left[-\frac{1}{2}\mathbf{s}^T(\boldsymbol{\kappa}_A + \boldsymbol{\kappa}_B)^{-1}\mathbf{s}\right], \tag{17}$$

where $\mathbf{s} = \mathbf{x}_A - \mathbf{x}_B$ is the distance between the particles at time $t = 0$. The convolution in (16) which yields (17) can be performed in Fourier space via the *Faltung* theorem [54]. Since $\boldsymbol{\kappa}_A = \boldsymbol{\kappa}_B = \boldsymbol{\kappa}$ we can rewrite (17) as

$$v(\mathbf{s},t) = \frac{\mathrm{Da}}{8\pi t\sqrt{1 + (\alpha t)^2/12}} \times \exp\left\{-\frac{\mathrm{Da}[|s|^2 - s_x s_y \alpha t + s_y^2(\alpha t)^2/3]}{8t[1 + (\alpha t)^2/12]}\right\}, \tag{18}$$

where $|s| = \sqrt{s_x^2 + s_y^2}$. We thus see that the collocation probability density (18) depends on the following parameters: (1) both components of $\mathbf{s}$, the initial interparticle distance, (2) the diffusion length scale $(2t/\mathrm{Da})^{1/2}$, and (3) the characteristic distance due to shear αt.

Assuming that the pair of A, B particles has survived over time t (i.e., they have not reacted with other particles), their probability to react with each other during the infinitesimal time $t' \in [t, t + dt)$ is given by

$$m_p v(\mathbf{s},t) dt, \tag{19}$$

where m_p is the nondimensional mass carried by a single particle, i.e., the number of moles multiplied by l^2/C_0. Thus, the probability of survival is given by the conditioned probability

$$P_s(t + dt) = P_s(t)[1 - m_p v(\mathbf{s},t) dt], \tag{20}$$

or, in words, the probability they are unreacted at $t + dt$ is the probability they were unreacted at t and did not react with each other since then. Hence,

$$dP_s/P_s = -m_p v(\mathbf{s},t) dt \tag{21}$$

and by integration over a time step t, we obtain the overall reaction probability of the couple during that time step,

$$P_r(t) = 1 - P_s(t) = 1 - \exp\left[-m_p \int_0^t v(\mathbf{s},t')\, dt'\right]. \tag{22}$$

For the degenerate case $\alpha = 0$, the integral in (22) yields

$$\int_0^t v(\mathbf{s},t')\, dt' = \frac{\mathrm{Da}}{8\pi} \mathrm{E}_1\left(\frac{\mathrm{Da}}{8t}|\mathbf{s}|^2\right), \tag{23}$$

where E_1 is the exponential integral. Note how this expression depends only on the absolute value of the interparticle distance, as the system becomes isotropic when $\alpha = 0$. For the general case $\alpha \neq 0$, Eq. (22) is integrated numerically (Fig. 2). However, the simplified solution (23) can be useful for approximating (22) when $(\alpha t)^2 \ll 12$. Hence, it can be used if the time steps are small enough (recall that t is the length of the time step in the framework of this section).

Also, with (23) it is easy to see that if $\frac{\mathrm{Da}}{8t} s^2 \to 0$, then the integral in (22) tends to infinity, and $P_r \to 1$. This comes as no surprise: when the particles are close by, or when they are given enough time to diffuse, their colocation probability is expected to be close to 1. If, on the other hand, $t \to 0$, while $\mathbf{s} \neq 0$, the collocation probability tends to a delta function in $\mathbf{s}$, and $P_r \to 0$. Again, this is expected since particles that are sufficiently far from one another cannot collocate unless they are given sufficient time to diffuse.

From a practical perspective to reduce numerical costs, the search for neighbors must be limited to a certain distance range. We define this range by the ellipse

$$\mathbf{s}^T(2\boldsymbol{\kappa})^{-1}\mathbf{s} = 2a^2, \tag{24}$$

where $a > 0$ is some predefined constant. Choosing larger a improves the accuracy of the numerical approach, but has an increased computational cost; as a rule of thumb, the choice $a = 2$ is typically sufficient as any induced error will be insignificantly small [51]. Note again that when $\alpha = 0$ the ellipse converges to a circle of radius $a\sqrt{8t/\mathrm{Da}}$.

With this cutoff search distance, the collocation probability (17) integrates to

$$\eta = 1 - e^{-a^2}, \tag{25}$$

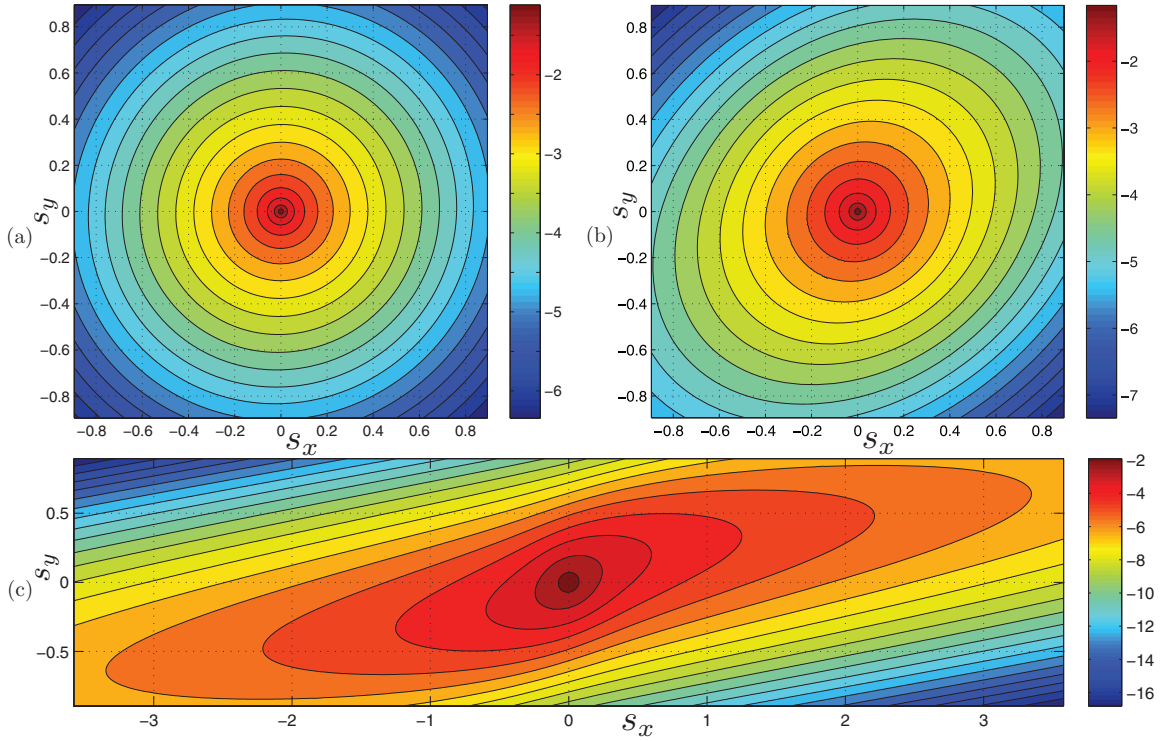

FIG. 2. (Color online) The integrated nondimensional collocation probability $\int_0^t v(\mathbf{s},t')\,dt'$ (in log scale) for $\mathrm{Da}/t = 1$ and $\alpha t = 0.1, 1, 10$ in (a), (b), (c), respectively.

so the collocation probability needs to be rescaled by the factor η^{-1} for consistency to ensure integration over the density to be unity. Hence, the probability of reaction of a single A particle during a time step is evaluated by numerical integration of (22), or by the first order approximation

$$P_r = \eta^{-1} m_p t \sum_{i=1}^{N_{nb}} v(\mathbf{s}_i, t), \tag{26}$$

where N_{nb} is the number of B neighbors found within the ellipse. The probability is compared to a random number generated from a uniform distribution $U \in [0,1]$. If $U > P_r$, the A particle under consideration is annihilated (removed from the system), and one of the neighboring B particles is annihilated as well. The choice between neighbors is done based on their weighted probability of reaction, so that we randomly choose the B particle based on its relative probability of reaction. Additionally, if a naïve search is performed to calculate collocation probabilities between all product pairs in the system, this can be computationally costly at $O(N^2)$, where N is the number of particles used. To speed up this process, we use an algorithm from the data mining literature called the kd tree [55], which accelerates this search to an $O(N \ln N)$ process, providing significant computational savings.

C. Numerical domain and finite size effects

The system we consider is idealized as ergodic and infinite. Therefore, the total mass in the system is infinite as well. Each particle represents a finite mass m_p. Hence, the number of particles needed to simulate the system accurately is infinite. This is clearly unfeasible since the number of particles in a numerical particle tracking simulation is finite and inherently constrained by the computational resources. To overcome this difficulty, we follow the classical approach of simulating the infinite system over a finite domain with periodic boundary conditions. At early times of the simulation, the finiteness of the domain is expected to have a negligible effect on the results and the domain can be considered infinite. However, at late times, boundary effects in the numerical simulation will lead to deviations from this idealization.

Indeed, previous works on purely diffusive transport [21,23,51] have observed and discussed this effect. For the case of no shear ($\alpha = 0$) over a domain of nondimensional size Ω^d with periodic boundary conditions, the finite size effects kick in when the typical size of segregated islands grows to about half of the domain size. This was observed around the time

$$t_{bnd} = \mathrm{Da}(\Omega/8)^2, \tag{27}$$

which can be thought of as representing the characteristic time of diffusion of concentration perturbations over the finite simulation domain. Similar if not more restrictive conditions will arise when $\alpha \neq 0$ and will be discussed in greater detail in the following. In this study, we use a rectangular domain $\mathcal{S} : [0,\Omega_x] \times [0,\Omega_y]$ for the numerical simulation.

D. Implementation of initial conditions

Implementing periodic boundary conditions in a numerical particle tracking method over a rectangular domain is

straightforward. The initial conditions (9)–(11) were implemented by randomly spreading N_0 particles of each species in the domain $\mathcal{S}$. The number of particles is not arbitrary, but rather is derived from the initial condition. Let us define the initial nondimensional density of particles by

$$\rho_0 = N_0/(\Omega_x \Omega_y). \tag{28}$$

This particle density is inversely proportional to the magnitude of the initial white noise μ and given by

$$\rho_0 = 1/\mu. \tag{29}$$

This expression is a straightforward extension of the one derived by Paster *et al.* [51, Appendix C]. To understand this result, consider a system where the initial condition for $C_i(\mathbf{x},t=0)$ is deterministic, i.e.,

$$C_A(\mathbf{x},t=0) = C_{A0}(\mathbf{x}), \quad C_B(\mathbf{x},t=0) = C_{B0}(\mathbf{x}), \tag{30}$$

such that $\mu \to 0$ (zero noise term). By (29), we find $\rho_0 \to \infty$. Hence, even if the domain is finite, an exact representation of the initial condition (30) necessitates the use an of *infinite* number of particles, which is consistent with classical random walk theory [56]. For such case, a particle tracking algorithm may be less favorable due the error induced by the finite number of particles.

In contrast, if we are interested in the case of a noisy or stochastic initial condition, as is the case with this work, this method might be regarded as ideal. For such cases, particle tracking methods require a finite number of particles for an accurate representation of the initial condition. When the initial condition contains a considerable noise, the reactive particle tracking method may be very efficient with regard to computational resources, due to the small number of initial particles needed. This may be an advantage over other numerical methods, such as Monte Carlo simulations using Eulerian finite difference, volume, or element methods. Additionally, random walk methods are known to be much less prone to numerical diffusion, which would lead to greater mixing and is thus an important factor in mixing-driven reactions [57].

V. RESULTS

Using the numerical algorithm described in the previous section, we have performed various simulations to study the effect of the Dahmköler number (Da) and shear rate (α) on the evolution of average concentration in the system (Table I). In Fig. 3, we show representative results for a specific Dahmköler number, namely Da = 2, spanning a range of α values (0, 10^{-4}, 10^{-3}, 10^{-2}, 10^{-1}, 1, 10). The figure also shows two analytical solutions, one corresponding to the well-mixed case, and an approximate analytical solution [51] that incorporates noisy initial conditions for $\alpha = 0$. A slight discrepancy between the numerical and the approximate analytical solution for $\alpha = 0$ is observed. As discussed in further detail in the following section, this discrepancy is due to restrictive assumptions involved in developing the analytical solution, namely, the neglecting of high-order moments of the concentration fluctuation fields.

TABLE I. Parameters of the numerical simulations. To speed up runs, the time step size is given by $\Delta t_j = \min\{\Delta t_{\max}, \Delta t_0(1+\epsilon)^j\}$, where j is the step number. For all simulations, $t_{bnd} = \mathrm{Da}N_0/64 = 5 \times 10^4$, the number of ensemble realizations was $N_{\mathrm{sim}} = 8$, the search radius factor was $a = 2$, and domain size was $\Omega_x \times \Omega_y = 1 \times 4$.

Da	α	N_0	Δt_0	ϵ	$\Delta t_{\max}$
2	0	6.4×10^6	2.5×10^{-3}	10^{-2}	50
	10^{-4}		2.5×10^{-3}	0.01	10
	10^{-3}		2.5×10^{-3}	0.01	10
	10^{-2}		2.5×10^{-3}	0.01	1
	10^{-1}		2.5×10^{-3}	0.01	1
	1		10^{-3}	2.5×10^{-3}	0.25
	10		2.5×10^{-4}	2.5×10^{-3}	0.05
8	0	1.6×10^6	0.025	0.025	100
	10^{-4}		0.025	0.025	100
	10^{-3}		0.025	0.025	100
	10^{-2}		0.025	0.025	10
	10^{-1}		0.025	0.025	10
	1		0.012	0.012	5
	10		0.012	0.012	1

A. Pure diffusion: $\alpha = 0$

First, to elucidate some matters, let us focus on the previously studied case of pure diffusion and no shear ($\alpha = 0$). The mean concentration curve for this case (see Fig. 3) matches the well-mixed solution at very early times, but clearly diverges from the well-mixed solution at relatively early times. This is consistent with the noisy initial condition for concentration, and has been extensively discussed in previous works (e.g., Paster *et al.* [51] and references therein). For this case, the only mixing mechanism is diffusion, which strives to homogenize the concentration field and drive the system to a well-mixed state. At the same time, reaction occurs in all locations where A and B coexist, thus annihilating A and B and promoting the segregation of species, destroying mixing in the system. Figure 4 depicts snapshots of particle locations at various times during the course of the simulation. These reveal that at very early times, A and B particles largely overlap in space and the system can be regarded as relatively well mixed. At later times, segregation leads to the formation of the aforementioned islands of single species, and reactions become restricted to their boundaries. At times for which island segregation is clearly visible, the average concentration in the domain scales with time as $t^{-1/2}$, in agreement with previous predictions and observations. As seen in Fig. 4, the total number of islands decreases with time, and the average size of an island grows respectively. Islands that contain significant mass of one species consume neighboring islands with lower mass of the second species, which in turn disappear from the system. At very late time, around $t \simeq t_{bnd}$ [see Eq. (27)], the finite size of the numerical domain starts to affect the simulation. At this time, the area occupied by a single island reaches

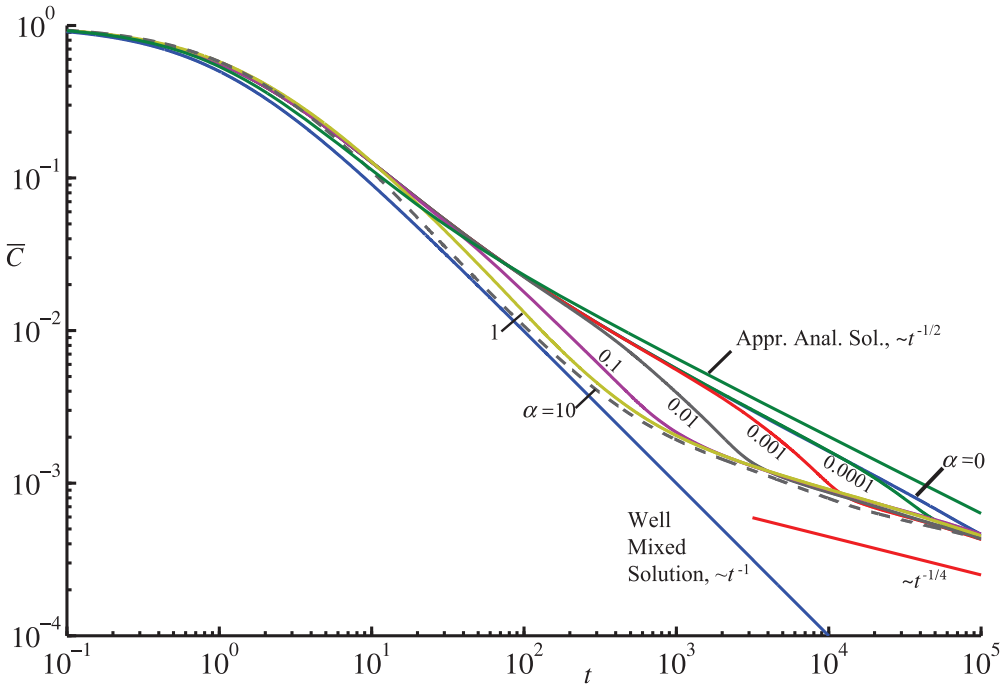

FIG. 3. (Color online) The evolution of mean concentration with time for Da = 2. The approximate analytical solution for $\alpha = 0$ and the well-mixed solution are also plotted. All parameters are nondimensional.

about half the domain area and the infinite-domain behavior breaks down. As noted above, for a detailed discussion on this see [51].

B. Diffusion and shear: $\alpha \neq 0$

For the cases where shear effects do exist (i.e., $\alpha \neq 0$), we observe a different behavior from the purely diffusive case, highlighting the role that shear plays in this system. Up to four discernible time regime scalings in average concentration emerge, which will be discussed in detail. First, we qualitatively describe the results.

At very early times, in all cases, there is a close agreement between the zero shear and finite shear simulations; at these earliest times diffusion dominates over shear effects and the latter are not discernible in the mean behavior of the system. At these times, the solutions break away from the well-mixed case and, other than for the highest simulated shear cases, all display the $t^{-1/2}$ regime. In the largest shear case ($\alpha = 10$), shear effects are strong enough to suppress this regime and the solution closely follows the well-mixed prediction, indicating that large shear can indeed suppress incomplete mixing effects. Then, at some α-dependent time, the solutions break away from this scaling and shift to a faster scaling of t^{-1}. The larger α, the earlier this transition occurs. During this time the concentration evolves parallel to the well-mixed solution, but at higher overall concentrations. Then again at some α-dependent value the solutions break away from this scaling and transition to another slower scaling of $t^{-1/4}$. This is a finite size effect associated with the horizontal size of the domain, which is unavoidable in a numerical study and can be explained theoretically (see Sec. VI), but is not expected in an infinite domain. All solutions collapse together during this regime, with deviations for different α values well within the standard deviation of the Monte Carlo simulation. Not surprisingly, we observed that increasing the number of realizations to calculate the average concentrations reduced the magnitude of these deviations. Since we are primarily interested in infinite-domain effects, we will focus on the regimes before the shear- and diffusion-induced boundary effects take place. Nonetheless, the latter warrant some further discussion.

Figure 4 shows particle locations at various times during the simulations for the Da = 2 case for multiple values of α. What is interesting to note is that at early times when the mean concentrations still match the $\alpha = 0$ case (see Fig. 3), the generic shapes of the islands look very similar to the $\alpha = 0$ case regardless of the specific value of α. However, as the breakaway from this regime occurs to the faster t^{-1} scaling, a noticeable difference appears, whereby the islands take on a different shape. At these times the islands are more elongated in one direction, which is tilted relative to the natural y axis, reflecting the presence of shear in the system and the fact that there is a superdiffusive growth along one axis and a diffusive one along the other. This is directly analogous to the fundamental solution of a point source in a diffusive shear flow in Eq. (13). It is at these times that the effect of the shear flow is important in the system.

Next, during the $t^{-1/4}$ regime (the finite size effect scaling), all islands now span the full horizontal extent of the domain. In essence, they have tilted all the way such that the superdiffusively growing axis is now closely aligned with the x axis. Reactions are now mostly limited by vertical diffusion across

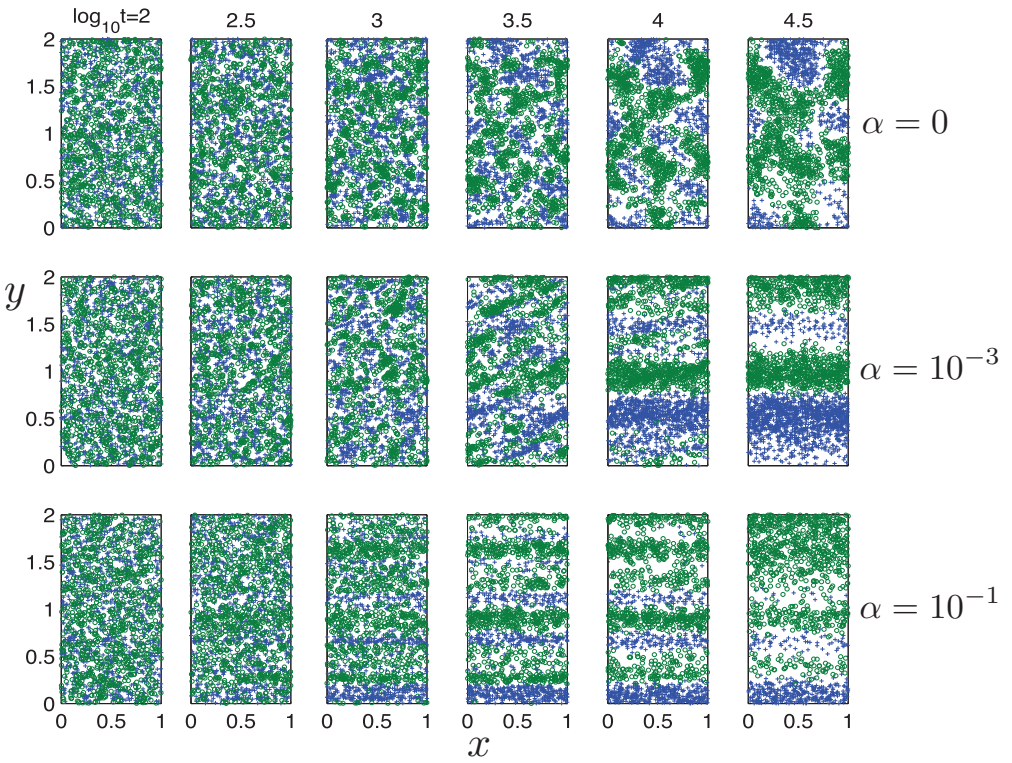

FIG. 4. (Color online) Evolution in time of some representative realizations with various shear rates, for Da = 2. Note how the islands form initially with irregular shape. Later on, for $\alpha > 0$, they tilt and become elongated due to the shear, and finally lie flat perpendicular to the x axis. Compare with Fig. 3. Note that, in the above figures, particle numbers were reduced (randomly) to $\sim 10^3$ to allow a good visualization of the results, and only the bottom half of the domain is shown.

islands and the system behaves as if it were one dimensional, which is consistent with an incomplete mixing scaling of $t^{-d/4}$ with d, the number of spatial dimensions, equal to one. This is a finite size effect associated with the time it takes for an island to span the horizontal width of the domain, unavoidable in a finite size numerical simulation, but not expected in an infinite domain (see the following section and Appendix B for more discussion and explanation on the matter).

Finally, at t_{bnd} [see Eq. (27)] another finite size effect, the same as in the cases with no shear, kicks in. At this point, the islands occupy half the domain; there is no longer any space for islands to grow as they would in an infinite domain, and a complete breakdown occurs. It is interesting to note that at the latest time in all the shear flow cases the islands are horizontally elongated, again reflecting the role of shear, while for the pure diffusion case it is equiprobable that they could be vertically or horizontally aligned, as there is no preferential direction for growth in a purely diffusive system.

Figure 5 shows the mean concentration against time for the same Da = 2 as well as Da = 8. This figure serves to highlight that qualitatively the behavior for both Da is very similar and all the observations and scalings discussed above still emerge. However, the breakaways from the well-mixed behavior and transitions between each of these scaling regimes occur at different times, indicating a Da-dependent behavior also. The emergence of these distinct time scalings is key to understanding incomplete mixing effects on chemical reactions, but at this point it is difficult to truly quantify these scalings from these observations alone. In the following (Sec. VI), the results will be interpreted using a semianalytical model that enables a more mechanistic explanation of each regime.

VI. INTERPRETATION OF SIMULATION RESULTS: A SEMIANALYTICAL CLOSURE

In this section, we present a semianalytical solution, based on methods from previous works that look at purely diffusive transport, to explain each of the time scaling regimes for mean concentration that were observed in Sec. V. This semianalytical approach is based on a closure argument. Similar closures have been invoked in many previous studies, but it should be noted that it is known to not be exact [18,21–23]. Rather, it enables one to predict the emergent scalings with time of mean concentrations, but not the exact values of mean concentration or time when these occur. Even in purely diffusive cases it is unable to match observations exactly without some empirical correction. These discrepancies have been studied and explained in detail by Paster *et al.* [51]. This is due to a problematic assumption behind the derivation of the closure, discussed in the following. Given these well-known limitations, our objective here is not to match exactly the observations from the numerical simulations, but to explore the emergent scalings with such a closure.

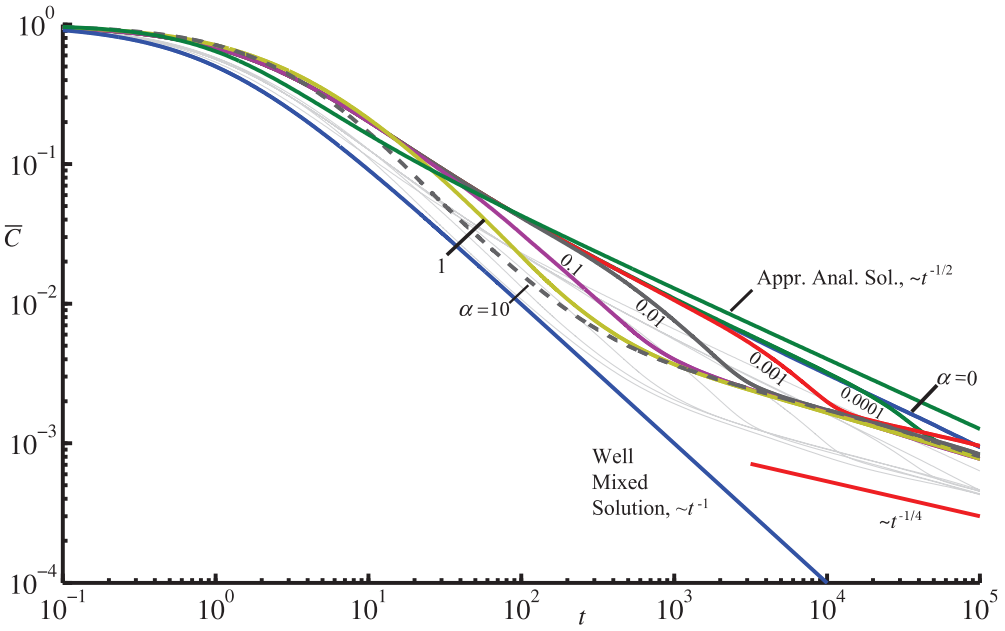

FIG. 5. (Color online) Same as Fig. 3 with additional solutions for Da = 8. The thin gray lines in the background correspond to the results for Da = 2.

A. Closure problem for mean concentrations

Averaging over Eqs. (1)–(3) it can readily be shown that the mean concentration of the reactants in this system will evolve based on the following ordinary differential equations:

$$\frac{d\overline{C_A}(t)}{dt} = \frac{d\overline{C_B}(t)}{dt} = -\overline{C_A}^2 - \overline{C'_A C'_B}. \tag{31}$$

Here, we have used the physical requirement that $\overline{C_A}(t) = \overline{C_B}(t)$ at all times since the initial condition is $\overline{C_A}(t=0) = \overline{C_B}(t=0)$ and the reaction stoichiometry is 1:1. When fluctuation concentrations are small relative to mean concentrations, the second term on the right hand side of (31) will be negligible and the system will evolve as is if it were well mixed. However, when the fluctuations are not small relative to mean concentrations this term plays an important role, changing the evolution of the system in a meaningful manner. This presents a closure problem as it requires a governing equation or model for the $\overline{C'_A C'_B}$ term.

To close this problem, we rely on previous works in diffusive and superdiffusive systems, where using the method of moments it has been shown that a reasonable closure is to assume

$$\overline{C'_A C'_B} = -\chi G(\mathbf{x} = \mathbf{x}_{\text{peak}}, t), \tag{32}$$

where G is the Green's function for conservative transport in the specified system, $\mathbf{x}_{\text{peak}}$ is the location of the peak of the Green's function, and χ is a constant. The formal derivation of closure (32) can be found in Refs. [21,23,58], where exact expressions for χ are developed. Similar closures without formal derivation have been proposed [18,22]. However, it is important to note that it relies on the assumption that moments higher than third order (i.e., terms that consist of products of three fluctuation concentrations) are negligible. While this is a standard assumption in many closure problems it is inaccurate as highlighted by Paster *et al.* [51], who showed that in diffusive systems the semianalytical solution and high resolution numerical solutions, while qualitatively similar in the late-time scaling, will behave differently. Indeed, using the "exact" values predicted by neglecting higher order moments [21,23] can in some instances yield unphysical results (e.g., creating rather than destroying mass of reactants when χ is too large). This mismatch is reconciled by demonstrating that third and higher order moments are in fact not negligible, but can have similar structure to second order moments, manifesting as a different effective value of χ [51]. This justifies the structure of closure (32), but not the specific value of χ predicted. Thus, for now, we keep χ as a free (constant) parameter in our closure.

B. Green's function for pure shear flow

The Green's function for transport in a pure shear flow, within our dimensionless framework, satisfies the following governing equation:

$$\frac{\partial G}{\partial t} + \alpha y \frac{\partial G}{\partial x} = \frac{1}{\text{Da}} \nabla^2 G \tag{33}$$

with natural boundary conditions at infinity and initial condition

$$G(\mathbf{x}, t=0) = \delta(\mathbf{x} - \mathbf{x}_0)\,, \tag{34}$$

in full analogy with the problem posed by (12), whose solution is given by (13). Thus,

$$G(\mathbf{x}=\mathbf{x}_{\text{peak}},t)=\frac{1}{2\pi\sqrt{\det[\boldsymbol{\kappa}]}}=\frac{\text{Da}}{2\pi t\sqrt{4+(\alpha t)^2/3}}. \quad (35)$$

Perhaps most notable in this solution is that for small α or small times the leading order behavior of $G(\mathbf{x}=\mathbf{x}_{\text{peak}},t)$ scales like t^{-1}, but at sufficiently large times, when the α-dependent term dominates in the denominator, the leading behavior scales like t^{-2}, which reflects the hypermixing regime alluded to earlier, where the plume spreads and the concentration peak decreases superdiffusively.

C. Solutions with the closure

With the proposed closure (32) and (35), our governing equation for the mean concentrations of the reactants (31) becomes

$$\frac{d\overline{C_A}(t)}{dt}=-\overline{C_A}^2+\frac{\chi\,\text{Da}}{2\pi t\sqrt{4+(\alpha t)^2/3}}. \quad (36)$$

While we are not aware of a closed form analytical solution to this equation for $\alpha\neq 0$, it is straightforward to integrate it numerically. Additionally, some useful asymptotic arguments can be made to understand how the solution evolves in time. These are discussed in the following subsection. Then, to show the full emergent behavior and verify our asymptotic arguments, we present numerical solutions of this equation. Note that for $\alpha=0$, Eq. (36) is a Riccati equation whose solution can be expressed in terms of Bessel functions [21,23].

Early times. At early times, if the background fluctuations in concentration are small relative to mean concentration, we expect the dominant balance in Eq. (36) to be between the term on the left hand side and the first term on the right hand side. In this case, the equation can be solved as

$$\overline{C_A}(t)=\frac{1}{1+t} \quad (37)$$

which is the solution for the well-mixed system.

Late times. As the concentrations deplete, the term $d\overline{C_A}/dt$ in Eq. (36) becomes negligible compared to the other terms in the equation. Then, the dominant balance in the equation shifts and becomes a balance between the two terms on the right hand side. Thus,

$$\overline{C_A}=\left(\frac{\text{Da}\chi}{2\pi t\sqrt{4+(\alpha t)^2/3}}\right)^{\frac{1}{2}}=\left(\frac{\text{Da}\chi}{4\pi}\right)^{\frac{1}{2}}(t^2+\alpha^2t^4/12)^{-\frac{1}{4}}. \quad (38)$$

Late-time scaling 1. Now, if at these times $t^2\gg\alpha^2t^4/12$, or $t<\sqrt{12}/\alpha$, then to leading order the concentration will decrease as $\overline{C_A}\sim t^{-1/2}$, which is the same scaling one would obtain for a purely diffusive system at late times in two dimensions. Note that for large values of α, this intermediate condition is not necessarily met since it may be violated when the incomplete mixing effects become important. Indeed, for the $\alpha=10$ cases presented in Fig. 5, this scaling never emerges.

Late-time scaling 2. At larger times when $\alpha^2t^4/12\gg t^2$, or $t>\sqrt{12}/\alpha$, the concentration will scale as $\overline{C_A}\sim t^{-1}$, which is the same scaling as if the system were well mixed. This suggests that the effect of a pure shear flow can indeed be strong enough to overcome the effects of incomplete mixing. However, the overall concentrations in the system could be considerably larger than the purely well-mixed case, due to the intermediate $\overline{C_A}\sim t^{-1/2}$ regime.

In a well-mixed system, the solution will evolve as $1/(1+t)$, which at late times approaches t^{-1}. Thus, we can define an asymptotic late-time retardation factor

$$R_{\text{asy}}=\left(\frac{2\pi\alpha}{\sqrt{3}\text{Da}\chi}\right)^{\frac{1}{2}}, \quad (39)$$

such that the concentration converges to $(R_{\text{asy}}t)^{-1}$, i.e., the influence of shear is to return the system to behaving in a manner reflective of perfect mixing, but at a later time. This is equivalent to having an effective (retarded) reaction rate $k_{\text{eff}}=k/R_{\text{asy}}$. While the notion of an effective reaction rate at these late times is useful, note that it should only be applied at late times when $t>\sqrt{12}/\alpha$.

Numerical solutions of semianalytical equation

In this section, we solve Eq. (36) numerically, using the numerical ordinary differential equation solver ODE23 available in MATLAB. From (36) it is evident that $\overline{C_A}(t)$ is a function of time depending on $\text{Da}\chi$ and α. Results varying and showing the respective influence of these are shown in Figs. 6 and 7.

In Fig. 6, we consider fixed $\text{Da}\chi$ and vary α over several orders of magnitude to demonstrate the influence of shear. In all cases at very early times we observe close agreement between the $\alpha=0$ incomplete mixing solution and the solutions with

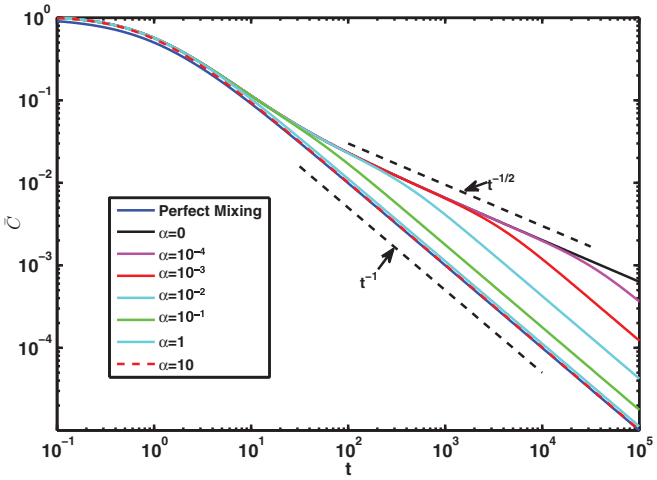

FIG. 6. (Color online) Numerical solution of (36) for various α, with fixed $\text{Da}\chi=5\times10^{-1}$. At late times, concentration scales like $t^{-1/2}$; at even later times, if $\alpha\neq0$, it scales like t^{-1}. The value of α affects the time of transition between each of the scaling regimes.

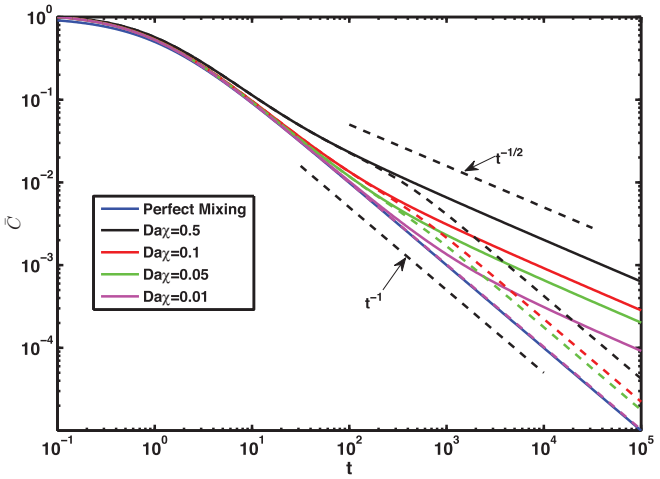

FIG. 7. (Color online) Numerical solution of (36) for various Daχ. In this figure, Daχ is varied to show how it affects the transition between each of the scaling regimes. The solid lines correspond to the equivalent case with no shear, i.e., $\alpha = 0$, and the dashed lines to $\alpha = 10^{-2}$.

shear. Then, again in all cases the solutions break away from this to a faster t^{-1} scaling as anticipated from the asymptotic arguments presented above. Larger α means an earlier breakaway to this faster regime. Note that the $\alpha = 10$ case never seems to follow the intermediate $t^{-1/2}$ regime, consistent with the idea that this regime need not occur if the conditions discussed above are not met.

In Fig. 7, we consider fixed α and vary Daχ. In this figure the solutions for each Daχ combination and $\alpha = 0$ are also shown. Raising Daχ triggers incomplete mixing effects at earlier times. Larger χ suggests larger noise in the initial condition, while larger Da means higher ratio of reaction to diffusion. When the product is larger, this means that fluctuations in the mean concentration will play an important role at earlier times. The effect of shear is to return from the $t^{-1/2}$ to a t^{-1} scaling. This is clearly seen for all cases and seems to occur at the same time, independent of Daχ, which is again consistent with the arguments in the previous section since this transition is determined solely by the value of α.

For both Figs. 6 and 7, we do not observe the late-time $t^{-1/4}$ scalings observed in the numerical simulations. As argued before, this scaling is a boundary effect due to the horizontal extent of the numerical domain, which an infinite-domain solution cannot reproduce. Since our primary interest here is the influence of the initial conditions on the late-time scaling of mean concentration in an infinite domain, we do not focus on the $t^{-1/4}$ scaling here. However, to demonstrate that it is truly a finite size effect associated with the limited horizontal extent of the domain, we extend the current closure to include finite boundary effect in Appendix B, which consistently demonstrates this behavior.

VII. CONCLUSIONS

In this work, we have studied mixing-limited reactions in a laminar pure shear flow to address the question of whether shear effects can overcome the effects of incomplete mixing on reactions. We have considered a simple spatial system, initially filled with equal amounts of two reactants A and B subjected to a background shear flow. The average concentrations of A and B are initially the same, but there are also background stochastic fluctuations in the concentrations. These can lead to long term deviations from well-mixed behaviors due to spatial segregation of the reactants, which can form isolated islands of individual reactants where reactions are limited to the island interfaces.

To study this system, we adapted a Lagrangian numerical particle-based random walk model, built originally to study mixing-driven bimolecular reactions in purely diffusive systems, to the case with a pure shear flow with the long term goal of developing it for more general nonuniform flows. Additionally, we studied the system theoretically by developing a semianalytical solution approach by proposing a simple closure argument. The results of the two approaches are qualitatively analogous in that the mean concentrations of reactants over time scale with the same power laws. An exact quantitative match, however, is not obtained; it is well known from previous work on diffusive transport that such closures are not exact, but that they can match emergent scalings in mean concentrations, which we demonstrate is also true for the case with shear considered here.

With both methods, we observed the following behaviors. At early times, when mean concentrations are much larger than background fluctuations, the system behaves as it if were well mixed. Then, when the fluctuations become comparable in size to the mean concentrations, and the domain becomes segregated, incomplete mixing slows down the reactions. Thus, the mean concentrations in the system evolve with a slower characteristic temporal scaling, consistent with a diffusion-limited case where shear is absent. Then, at later times when shear effects begin to dominate, the system returns to behaving in a manner similar to a perfectly mixed system, but described by an overall lower effective reaction rate constant. If shear is sufficiently strong, the diffusivelike incomplete mixing regime never emerges and the system behaves as well mixed at all times. It is important to note that this does not mean that the system is actually well mixed as segregated islands still occur, but rather that the mixing associated with the shear flow is sufficiently fast to result in a scaling analogous to a well-mixed system.

The system is characterized by two dimensionless numbers. Da is a Damköhler number that quantifies the relative magnitude of reaction time scales to diffusion time scales. Large Da means that reactions happen more quickly than diffusion can homogenize any background fluctuations; thus, systems with larger Da will amplify initial fluctuations and incomplete mixing patterns can play an important role at late times. Likewise, when Da is small, diffusion can homogenize fluctuations more quickly and the system will behave as better mixed. The second dimensionless number is α, a dimensionless shear rate that quantifies relative influence of shear to reaction. The Damköhler influences the onset time of incomplete mixing, while α controls the onset of a return to well-mixed type scaling.

A key take home message of this work is that, while a pure shear flow can lead to a behavior that is consistent with a well-mixed system, if the nature and evolution of

incomplete mixing in the system is not adequately accounted for, then predictions of reactant concentrations, particularly at late times, can be off by as much as orders of magnitude. In contrast, if incomplete mixing is accounted for, more realistic predictions can be obtained.

ACKNOWLEDGMENTS

P.A. would like to acknowledge partial funding by the Startup grant of the V.P. of research in TAU. T.A. gratefully acknowledges support by the Portuguese Foundation for Science and Technology (FCT) under Grant No. SFRH/BD/89488/2012. D.B. would like to acknowledge partial funding via NSF Grants No. EAR-1351625 and No. EAR-1417264 as well as the U. S. Army Research Laboratory and the U. S. Army Research Office under Contract/Grant No. W911NF1310082. The authors thank the two anonymous reviewers for their constructive comments on the manuscript.

APPENDIX A: EXPRESSIONS FOR THE EIGENVALUES AND EIGENVECTORS OF $\boldsymbol{\kappa}$

The eigenvalues of $\boldsymbol{\kappa}$, the covariance matrix, are given by

$$\lambda_{1,2} = \tfrac{1}{2}\{\mathrm{Tr}(\boldsymbol{\kappa}) \pm \sqrt{[\mathrm{Tr}(\boldsymbol{\kappa})]^2 - 4\det\boldsymbol{\kappa}}\}, \tag{A1}$$

where

$$\mathrm{Tr}(\boldsymbol{\kappa}) = \kappa_{11} + \kappa_{22} = \frac{4t}{\mathrm{Da}}\left[1 + \frac{1}{6}\alpha^2 t^2\right] \tag{A2}$$

is the trace of $\boldsymbol{\kappa}$ and

$$\det\boldsymbol{\kappa} = \kappa_{11}\kappa_{22} - \kappa_{12}^2 = \frac{4t^2}{\mathrm{Da}^2}\left[1 + \frac{1}{12}\alpha^2 t^2\right]. \tag{A3}$$

Substituting (A2) and (A3) into (A1) one finds

$$\lambda_{1,2} = \frac{2t}{\mathrm{Da}}\left\{1 \pm \left[\frac{1}{2}\alpha t\sqrt{1 + \frac{1}{9}(\alpha t)^2}\right] + \frac{1}{6}\alpha^2 t^2\right\}. \tag{A4}$$

The eigenvectors, in turn, are aligned with

$$\mathbf{v}'_{1,2} = \begin{bmatrix} 1 \\ -\frac{1}{3}\alpha t \pm \sqrt{1 + \frac{1}{9}(\alpha t)^2} \end{bmatrix} \tag{A5}$$

and the normalized unit vectors $\mathbf{v}_{1,2}$ are readily obtained by normalization of $\mathbf{v}'_{1,2}$.

When $\alpha t \ll 1$, the eigenvectors are inclined at about $\pm 45^\circ$ relative to the $\hat{x}$ axis. For larger αt, the eigenvectors tilt clockwise (see Fig. 1), and for $\alpha t \gg 1$, they tend to align with $\hat{x}$ and $-\hat{y}$ or, more precisely, with $[1, 3/(2\alpha t)]$ and $(1, -\frac{2}{3}\alpha t)$.

In practice, the new location of a particle can be obtained by translation of the x coordinate of the particle by $\alpha y_0 t$, and a random walk in two dimensions with jumps along the rotated eigenvectors of $\boldsymbol{\kappa}$ with magnitudes

$$\begin{aligned} x_1 &= \xi_1\sqrt{\lambda_1}, \\ x_2 &= \xi_2\sqrt{\lambda_2}, \end{aligned} \tag{A6}$$

where x_i is the walk length in the direction of the ith eigenvector, and ξ_i is a random number, generated from a normal distribution with zero mean and unit variance. Hence, the new location is given by

$$\begin{aligned} x &= x_0 + \alpha y_0 t + \sum_{i=1}^{d}(\mathbf{v}_i \cdot \hat{x})x_i, \\ y &= y_0 + \sum_{i=1}^{d}(\mathbf{v}_i \cdot \hat{y})x_i. \end{aligned} \tag{A7}$$

APPENDIX B: DOMAIN BOUNDARY EFFECTS

As discussed in Sec. VI, we wish to demonstrate that the $t^{-1/4}$ scaling can be attributed to a boundary effect. Specifically, we will argue here that this scaling is associated with finite extent of the horizontal boundaries of the domain. As shown in Eq. (32), the evolution of the mean concentration depends on the peak of the Green's function for conservative transport. For a finite periodic domain this can be be calculated by the method of images

$$G(\mathbf{x} = \mathbf{x}_{\mathrm{peak}}, t) = \sum_{n=-\infty}^{\infty} \frac{1}{(2\pi)^{d/2}\sqrt{\det[\boldsymbol{\kappa}]}} \exp\left[-\frac{1}{2}\xi_n^T \boldsymbol{\kappa}^{-1}\xi_n\right], \tag{B1}$$

where

$$\xi_n = (n\Omega_x, 0) \tag{B2}$$

and Ω_x is the horizontal length of the domain. In essence, this solution adds every contribution from point plumes located at equidistant intervals of Ω_x along the x axis at $y = 0$ and sums their contribution to the point $x = 0$, which is where the peak of the Green's function for a point source located initially at $(x, y) = (0, 0)$ will occur. It is convenient to take this point as one does not have to account for advection-induced drift in the peak location, but the result is independent of this choice. We have

$$G(\mathbf{x} = \mathbf{x}_{\mathrm{peak}}, t) = \frac{\mathrm{Da}}{4\pi t\sqrt{1 + \alpha^2 t^2/12}} \times \sum_{n=-\infty}^{\infty} \exp\left[-\frac{\mathrm{Da}(n\Omega_x)^2}{4t(1 + \alpha^2 t^2/12)}\right] \tag{B3}$$

which at late times converges to

$$G(\mathbf{x} = \mathbf{x}_{\mathrm{peak}}, t) = \frac{\sqrt{3}}{2\pi}\frac{\mathrm{Da}}{|\alpha| t^2} \sum_{n=-\infty}^{\infty} \exp\left[-\frac{3\mathrm{Da}(n\Omega_x)^2}{\alpha^2 t^3}\right]. \tag{B4}$$

The term outside of the summation scales like t^{-2}, as for the infinite-domain case. As $t^3 \gg 3\mathrm{Da}\Omega_x^2/\alpha^2$ when the boundary effects become important, the infinite sum can be approximated by an integral which converges to

$$\sqrt{\frac{\pi}{3\mathrm{Da}}}\frac{|\alpha|}{\Omega_x} t^{3/2}. \tag{B5}$$

Thus, the Green's function converges to

$$G(\mathbf{x} = \mathbf{x}_{\mathrm{peak}}, t \to \infty) = \frac{1}{2}\sqrt{\frac{\mathrm{Da}}{\pi}}\frac{1}{\Omega_x} t^{-1/2}. \tag{B6}$$

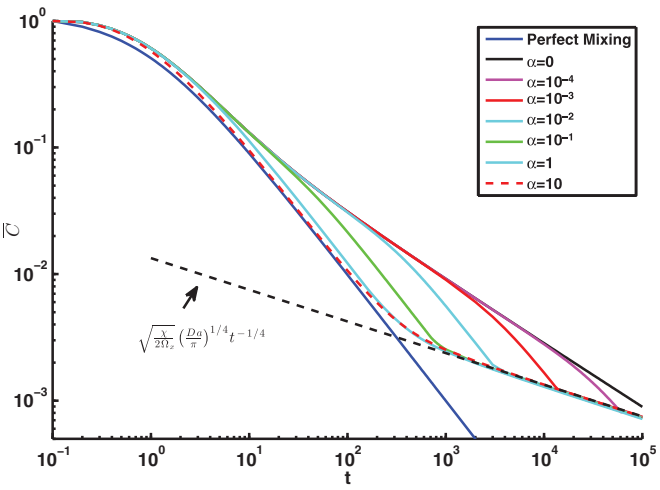

FIG. 8. (Color online) Numerical solution for the average concentration using the finite-domain Green's function in Eq. (B1) for various α, Da $= 10$, and $\chi = 0.01$. In this figure, α is varied to show how it affects the transition between each of the scaling regimes. Note the collapse of all late-time scalings on to the same line $\overline{C}_i(t) = \sqrt{\frac{\chi}{2\Omega_x}}\left(\frac{\mathrm{Da}}{\pi}\right)^{1/4} t^{-1/4}$, in agreement with observations from numerical simulations.

Hence, the combined effect on the scaling of the peak of the Green's function is

$$G(\mathbf{x} = \mathbf{x}_{\mathrm{peak}}, t) \sim t^{-1/2}. \tag{B7}$$

Since at late times our dominant balance argument indicates that $\overline{C}_i = \sqrt{\chi G(\mathbf{x} = \mathbf{x}_{\mathrm{peak}}, t)}$, once the horizontal boundary effects are felt, the mean concentrations will converge to

$$\overline{C}_i(t) = \sqrt{\chi G(\mathbf{x}_{\mathrm{peak}}, t)} = \sqrt{\frac{\chi}{2\Omega_x}}\left(\frac{\mathrm{Da}}{\pi}\right)^{1/4} t^{-1/4} \tag{B8}$$

which is independent of the value of α, and scales like $t^{-1/4}$. These results are in agreement with the observations in the particle tracking simulations. In Fig. 8, we plot the evolution of the average concentration over time by solving Eqs. (31) and (32) numerically, using the finite-domain Green's function in (B3), instead of its infinite-domain counterpart.

The results in the figure are very similar to those observed in the numerical simulations, particularly in that at late times all solutions for $\alpha \neq 0$ collapse on to the same curve. This scaling can also be interpreted physically as a boundary effect as follows. At the relevant late times, the single-reactant islands span the full width of the domain and the system essentially becomes one dimensional. The late-time incomplete-mixing scaling is known to behave as $t^{-d/4}$, which matches our findings [18]. This again demonstrates the utility of the simple proposed closure in interpreting the results observed in the numerical simulations. As a cautionary note, we would again like to highlight that the proposed closure is not exact; the good agreement with simulations is promising, but further work is required to refine it rigorously.

[1] J. Seinfeld and S. Pandis, *Atmospheric Chemistry and Physics: From Air Pollution to Climate Change* (Wiley, Hoboken, NJ, 2006).
[2] I. Mezić, S. Loire, V. Fonoberov, and P. Hogan, Science **330**, 486 (2010).
[3] C. Escauriaza, C. Gonzalez, P. Guerra, P. Pasten, and G. Pizarro, Bull. Am. Phys. Soc. **57**, 13005 (2012).
[4] P. Znachor, V. Visocká, J. Nedoma, and P. Rychtecký, Freshwater Biol. **58(9)**, 1889 (2013).
[5] J. Sierra-Pallares, D. L. Marchisio, E. Alonso, M. T. Parra-Santos, F. Castro, and M. J. Cocero, Chem. Eng. Sci. **66(8)**, 1576 (2011).
[6] W. Stockwell, Meteorol. Atmos. Phys. **57**, 159 (1995).
[7] L. Whalley, K. Furneaux, A. Goddard, J. Lee, A. Mahajan, H. Oetjen, K. Read, N. Kaaden, L. Carpenter, A. Lewis *et al.*, Atmos. Chem. Phys. **10**, 1555 (2010).
[8] T. Michioka and S. Komori, AIChE Journal **50**, 2705 (2004).
[9] J. Pauer, K. Taunt, W. Melendez, R. Kreis Jr., and A. Anstead, J. Great Lakes Res. **33**, 554 (2007).
[10] C. Gramling, C. Harvey, and L. Meigs, Environ. Sci. Technol. **36**, 2508 (2002).
[11] M. de Simoni, J. Carrera, X. Sanchez-Vila, and A. Guadagnini, Water Resour. Res. **41**, W11410 (2005).
[12] P. d. Anna, J. Jimenez-Martinez, H. Tabuteau, R. Turuban, T. Le Borgne, M. Derrien, and Y. Mheust, Environ. Sci. Technol. **48**, 508 (2014).
[13] P. De Anna, M. Dentz, A. Tartakovsky, and T. Le Borgne, Geophys. Res. Lett. **41**, 4586 (2014).
[14] M. Dentz and J. Carrera, Phys. Fluids **19**, 017107 (2007).
[15] D. Gillespie, J. Chem. Phys. **113**, 297 (2000).
[16] A. Ovchinnikov and Y. Zeldovich, Chem. Phys. **28**, 215 (1978).
[17] D. Toussaint and F. Wilczek, J. Chem. Phys. **78**, 2642 (1983).
[18] K. Kang and S. Redner, Phys. Rev. Lett. **52**, 955 (1984).
[19] E. Monson and R. Kopelman, Phys. Rev. Lett. **85**, 666 (2000).
[20] E. Monson and R. Kopelman, Phys. Rev. E **69**, 021103 (2004).
[21] A. M. Tartakovsky, P. de Anna, T. Le Borgne, A. Balter, and D. Bolster, Water Resour. Res. **48**, W02526 (2012).
[22] G. Zumofen, J. Klafter, and M. F. Shlesinger, Phys. Rev. Lett. **77**, 2830 (1996).
[23] D. Bolster, P. de Anna, D. A. Benson, and A. M. Tartakovsky, Adv. Water Resour. **37**, 86 (2012).
[24] R. Klages, I. Radons, and Gand Sokolov, *Anomalous Transport: Foundations and Applications* (Wiley, Hoboken, NJ, 2008).
[25] D. Koch and J. Brady, J. Fluid Mech. **180**, 387 (1987).
[26] D. Koch and J. Brady, Phys. Fluids **31**, 965 (1988).
[27] D. Koch, R. Cox, H. Brenner, and J. Brady, J. Fluid Mech. **200**, 173 (1989).
[28] F. Boano, A. I. Packman, A. Cortis, R. Revelli, and L. Ridolfi, Water Resour. Res. **43**, W10425 (2007).
[29] B. Berkowitz, A. Cortis, M. Dentz, and H. Scher, Rev. Geophys. **44**, RG2003 (2006).
[30] D. Benson and S. Wheatcraft, Transport Porous Media **42**, 211 (2001).
[31] F. Höfling and T. Franosch, Rep. Prog. Phys. **76**, 046602 (2013).
[32] S. Jones and W. Young, J. Fluid Mech. **280**, 149 (1994).

[33] C. Escauriaza and F. Sotiropoulos, J. Fluid Mech. **641**, 169 (2009).
[34] H. Aref and S. Balachandar, Phys. Fluids **29**, 3515 (1986).
[35] T. H. Solomon and J. P. Gollub, Phys. Rev. A **38**, 6280 (1988).
[36] Z. Pouransari, M. Speetjens, and H. Clercx, J. Fluid Mech. **654**, 5 (2010)
[37] M. Latini and A. Bernoff, J. Fluid Mech. **441**, 399 (2001).
[38] P. Shankar, J. Fluid Mech. **631**, 363 (2009).
[39] A. Okubo, J. Oceanogr. Soc. Jpn. **24**, 60 (1968).
[40] A. Okubo and M. J. Karweit, Limnol. Oceanogr. **14**(4), 514 (1969).
[41] E. Novikov, J. Appl. Math. Mech. **22**, 576 (1958).
[42] G. Csanady, *Turbulent Diffusion in the Environmnet*, Geophysics and Astrophysics Monographs, Vol. 3 (Reidel, Dordrecht, 1973), pp. 147–148.
[43] H. Tennekes and J. L. Lumley, *A First Course in Turbulence* (MIT Press, Cambridge, MA, 1972).
[44] A. Monin and A. Yaglom, *Statistical Fluid Mechanics: Mechanics of Turbulence*, Vol. 1 (Dover, New York, 2007).
[45] D. Bolster, M. Dentz, and T. Le Borgne, Water Resourc. Res. **47**, W09602 (2011).
[46] S. Pope, *Turbulent Flows* (Cambridge University Press, Cambridge, UK, 2000).
[47] T. LeBorgne, M. Dentz, D. Bolster, J. Carrera, J. deDreuzy, and P. Davy, Adv. Water Resourc. **33**, 1468 (2010).
[48] P. Kitanidis, Water Resourc. Res. **30**, 2011 (1994).
[49] F. de Barros, M. Dentz, J. Koch, and W. Nowak, Geophys. Res. Lett. **39**, L08404 (2012).
[50] D. A. Benson and M. M. Meerschaert, Water Resourc. Res. **44**, W12201 (2008).
[51] A. Paster, D. Bolster, and D. A. Benson, J. Comput. Phys. **263**, 91 (2014).
[52] D. Bolster, M. Dentz, and J. Carrera, Water Resourc. Res. **45**, W05408 (2009).
[53] A. Paster, D. Bolster, and D. A. Benson, Water Resourc. Res. **49**, 1 (2013).
[54] G. Dagan, *Flow and Transport in Porous Formations*, Vol. 804 (Springer, New-York, 1989).
[55] K. Candan and M. Sapino, *Data Management for Multimedia Retrieval* (Cambridge University Press, Cambridge, UK, 2010).
[56] H. Risken, *Fokker-Planck Equation* (Springer, New York, 1984).
[57] D. Benson, D. Bolster, N. Engdahl, and T. Aquino (unpublished).
[58] A. Paster and D. Bolster, Physica A (Amsterdam) **391**, 4654 (2012).